Ground-state phase diagram and magnetoconductance of a one-dimensional Hubbard superlattice at half filling

Jayeeta Chowdhury,[1] S. N. Karmakar,[2] and Bibhas Bhattacharyya[3]
[1]*Department of Physics, East Calcutta Girls' College, Lake Town, Lake Town Link Road, Kolkata 700 089, India*
[2]*TCMP Division, Saha Institute of Nuclear Physics, 1/AF Bidhannagar, Kolkata 700 064, India*
[3]*Department of Physics, Scottish Church College, 1 and 3 Urquhart Square, Kolkata 700 006, India*
(Received 28 March 2007; published 21 June 2007)

We have studied a one-dimensional Hubbard superlattice with different Coulomb correlations at alternating sites for a half-filled band. Mean field calculations based on the Hartree-Fock approximation together with a real space renormalization group technique were used to study the ground state of the system. The phase diagrams obtained in these approaches agree with each other from the weak to the intermediate coupling regime. The mean field results show very quick convergence with system size. The renormalization group results indicate a spatial modulation of local moments that was identified in some previous work. Also we have studied the magnetoconductance of such superlattices which reveals several interesting points.

DOI: 10.1103/PhysRevB.75.235117 PACS number(s): 71.30.+h, 73.21.Cd, 71.45.Lr, 75.30.Fv

I. INTRODUCTION

The study of electronic correlation remains at the focus of recent theoretical interest due to the development of different materials of which the metallic multilayers[1] form a very important component. The oscillation of exchange coupling between magnetic layers[2] and the appearance of giant magnetoresistance[3] are among the exciting features of the magnetic multilayers, e.g., the layered Fe/Cr structures. An intense theoretical attempt has been made to understand the magnetic behavior of such systems.[4–8] In these pioneering works in this field a simple generalization of the one-dimensional Hubbard model was proposed to investigate the role of electronic correlation in one-dimensional superlattices. This model consists of a periodic arrangement of N_U sites in which the on-site Coulomb correlation (U) is repulsive followed by N_0 sites with no on-site interaction ($U=0$). It was found that such a model gives rise to some interesting features, in sharp contrast with the magnetic behavior observed in an otherwise homogeneous system (conventional one band Hubbard model).[4]

However, most of the previous works in this model employed exact diagonalization of finite systems typically having 8–24 sites.[4,5] Some of these works reveal preferential distribution of local moments on sublattices and observe the suppression of spin-density-wave (SDW) order.[4] Some others deal with problems like metal-insulator transition (MIT) (Ref. 5) or formation of charge density wave[6] in such systems. Density matrix renormalization group (DMRG) calculations are also performed to overcome limitations on system size imposed by the technique of exact diagonalization; and, these consider system sizes ~48–150.[7] Very recently a generalization of the said model has been considered where, instead of two types of sites with on-site correlation parameters $U>0$ and $U=0$, respectively, one takes into account two different values of $U(>0)$ at adjacent sites;[9] however, a detailed study of this generalized model is yet to be worked out. In view of the wider applicability of this model to diverse experimental systems, we consider here a preliminary study of this alternating Hubbard model (AHM) in one dimension. Also we aim at observing the behavior of the same when the system size is reasonably large.

In the present study, we investigate the ground-state properties of the AHM in one dimension and for a half-filled band by using a Hartree-Fock approximation (HFA) together with a real space renormalization group (RG) calculation. These two techniques, complemented by one another, were found to be very successful in studying similar cases in the recent past.[10] Apart from constructing the ground-state phase diagram we also investigate the magnetoconductance of a finite chain within the HFA scenario. In Sec. II we introduce the model and give the HFA calculations. Section III describes the results obtained in HFA. Section IV contains some details of the RG scheme while Sec. V shows the RG results together with a comparison between the same and that obtained in the HFA. In Sec. VI we present the results on magnetoconductance of the model and Sec. VII summarizes the present work.

II. THE MODEL AND THE HARTREE-FOCK CALCULATIONS

Our model is defined on a one-dimensional Hubbard chain of N (even integer) sites consisting of two sublattices. The model Hamiltonian is

$$H = t\sum_{i,\sigma}(c^{\dagger}_{i,\sigma}c_{i+1,\sigma} + \text{H.c.}) + U_A\sum_{i\in\mathcal{A}} n_{i,\uparrow}n_{i,\downarrow} + U_B\sum_{i\in\mathcal{B}} n_{i,\uparrow}n_{i,\downarrow}. \tag{1}$$

The two sublattices constructed out of odd and even numbered sites are labeled by $\mathcal{A}$ and $\mathcal{B}$, respectively. $c^{\dagger}_{i,\sigma}(c_{i,\sigma})$ is the creation (annihilation) operator for an electron with spin σ at the ith site. $n_{i,\sigma}=c^{\dagger}_{i,\sigma}c_{i,\sigma}$, and $n_i=\Sigma_\sigma n_{i,\sigma}$ is the number operator at the ith site. t is the hopping integral between nearest-neighbor sites. U_A, U_B are the on-site Coulomb repulsion energies on the sites corresponding to two sublattices $\mathcal{A}$ and $\mathcal{B}$, respectively.

We decouple the Hamiltonian within the HFA, which is expected to work at least in the weak coupling regime. We

define two parameters, number of electron N_i and the magnetization M_i at the ith site, where

$$N_i = \langle n_{i,\uparrow} \rangle + \langle n_{i,\downarrow} \rangle,$$

$$M_i = \langle n_{i,\uparrow} \rangle - \langle n_{i,\downarrow} \rangle. \quad (2)$$

These lead to a decoupled Hamiltonian,

$$H = t\sum_{i,\sigma} (c^{\dagger}_{i,\sigma} c_{i+1,\sigma} + \text{H.c.}) + \frac{U_A}{2} \sum_{i \in \mathcal{A}} [(N_i + M_i) n_{i,\downarrow} + (N_i - M_i) n_{i,\uparrow}] + \frac{U_B}{2} \sum_{i \in \mathcal{B}} [(N_i + M_i) n_{i,\downarrow} + (N_i - M_i) n_{i,\uparrow}] - \frac{1}{4}(U_A + U_B)(N_i^2 - M_i^2). \quad (3)$$

Now the Hamiltonian can be divided into two parts for two types of spins, i.e., $H = H_{\uparrow} + H_{\downarrow}$. In an unrestricted HFA one diagonalizes $H_{\uparrow}$ and $H_{\downarrow}$ in a self-consistent manner to obtain the single particle energy levels. The ground state can be constructed by filling up the energy levels from both the up and the down bands up to the Fermi level.

One can define the spin and the charge density order parameters, c and s, respectively, by

$$c = \frac{1}{N}\sum_i (-1)^i (n_{i,\uparrow} + n_{i,\downarrow}), \quad s = \frac{1}{N}\sum_i (-1)^i (n_{i,\uparrow} - n_{i,\downarrow}).$$

We consider a half-filled chain with periodic boundary condition. One can easily check by using an unrestricted HFA calculation that all sites corresponding to a given sublattice become equivalent under a periodic boundary condition. This leads to a simplification of the formulas for c and s given above. We, therefore, use these simplified forms of the charge density order parameter c and the spin-density order parameter or antiferromagnetic order parameter s as given by

$$c = \tfrac{1}{2}\langle n_{B,\uparrow} + n_{B,\downarrow} - n_{A,\uparrow} - n_{A,\downarrow} \rangle,$$

$$s = \tfrac{1}{2}\langle n_{B,\uparrow} - n_{B,\downarrow} - n_{A,\uparrow} + n_{A,\downarrow} \rangle. \quad (4)$$

It is to be noted here that $|c| = 1$ for a perfect "chess-board"-type CDW and $|s| = 1$ for a perfect Néel-type antiferromagnetic SDW state. We now investigate the dependence of these order parameters on the values of U_A and U_B.

III. THE RESULTS OF HARTREE-FOCK CALCULATIONS

In Fig. 1 we plot the order parameters c and s as functions of U_B/t for different fixed values of U_A/t (for a chain having sites $N=100$). Keeping U_A/t at a fixed value (>0) and varying U_B/t from 0 to higher values, we find that initially the system is charge ordered. The electrons tend to localize at the sites with lower Coulomb repulsion energies, keeping the other sites vacant. As a result a charge-density wave (CDW) is formed. In this regime, the charge-density order parameter c assumes a high value while the spin-density order parameter s is zero. As we gradually increase U_B/t keeping U_A/t at the same fixed value, we see that there is a gradual fall in the value of c. At a certain value of U_B/t there occurs a sharp rise in s which now takes over the value of c. For small values of $U_A/t (\ll 1)$ the transition occurs at the point of homogeneity, i.e., at $U_B = U_A$. In this case, however, a further increase in U_B/t suppresses the spin order again, and the CDW sets in. Therefore, the SDW is found to form only at a singular point $U_A = U_B$ which is in agreement with the known result for the "homogeneous" limit.[11] The situation becomes different for larger values of U_A/t. For an intermediate value of $U_A/t (\sim 1)$, we find two transitions: one from a CDW to an SDW and then from the SDW to a CDW again; this can be identified by two successive crossovers in the c and the s curves [Fig. 1(b)]. It is interesting to note that the charge order vanishes only at the point of homogeneity. For large $U_A/t (\gg 1)$ there appears only one transition from a CDW state to an SDW state at a specific value of $U_B/t (< U_A/t)$. Here also, the charge-order parameter vanishes at $U_A = U_B$, and then rises slowly with $U_B/t (> U_A/t)$. However, in this region, the spin-order parameter always dominates over the charge-order parameter [Fig. 1(c)]. The phase transitions occurring at points of crossovers of c and s can further be explored by studying the gap in the spectrum at the Fermi level. The energy gap Δ_{HFA} at the Fermi level of a system containing n electrons can be estimated from

$$\Delta_{\text{HFA}} = E_{n+1} - E_n,$$

where, E_n is the ground-state energy of (3) for a system of n particles. In Fig. 2 we plot the energy gap Δ_{HFA} as a function of U_B/t for different fixed values of U_A/t at half filling. Dips in the curves of Δ_{HFA} match with the corresponding values of U_B/t that were identified as points of phase transitions in Fig.

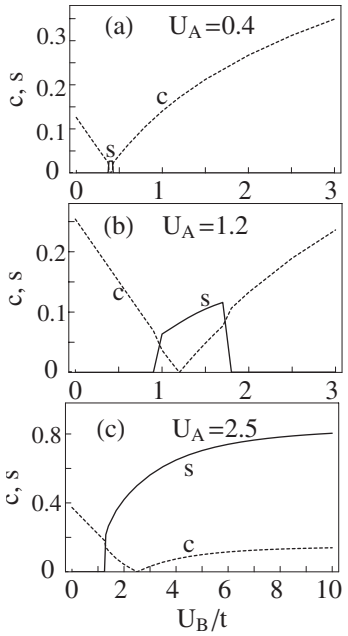

FIG. 1. Plot of the order parameters c and s as functions of U_B/t for (a) $U_A=0.4$, (b) $U_A=1.2$, and (c) $U_A=2.5$ (scale of energy is chosen by setting $t=1.0$) for $N=100$. The dotted line corresponds to the charge-order parameter c while the solid line shows the spin-order parameter s as calculated from HFA.

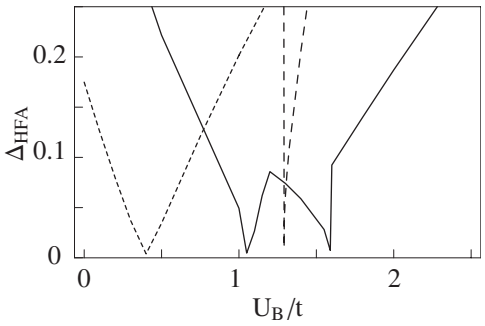

FIG. 2. Plot of the energy gap Δ_{HFA}, as found from HFA, as a function of U_B/t for $N=300$. We have used the dotted line for $U_A=0.4$, the solid line for $U_A=1.2$, and the dashed line for $U_A=2.5$ (scale of energy is chosen by setting $t=1.0$). Note that the zeroes in the gap match with the transition points identified from Fig. 1.

1. It is to be noted here that for large values of U_A/t the energy gap sharply increases after the CDW-SDW transition has occurred (Fig. 2). In this regime the slow increase of the charge-order parameter does not modify this behavior.

Identification of the points of phase transitions by the methods mentioned above enables us to draw the phase diagram of the model (1) on the U_A/t-U_B/t plane within the HFA. In Fig. 3 we plot the phase diagrams for different N values to note the quick convergence of the present mean field results with system size. For small values of U_A and U_B the antiferromagnetic phase actually occurs along the line of "homogeneity" ($U_A=U_B$). For higher values of U_A and U_B we obtain a centrally located broad SDW region together with two charge-ordered phases located near the axes. The phase diagram turns out to be perfectly symmetric about the line of homogeneity along which the system is already known to be antiferromagnetic from exact calculations.[11] In the limit $U_B \gg U_A$ ($U_A \gg U_B$) the CDW-SDW transition line above (below) the line of homogeneity bends towards the U_B/t (U_A/t) axis.

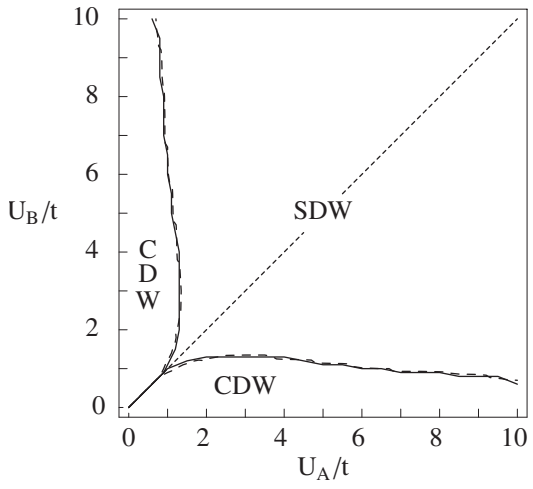

FIG. 3. The HFA phase diagram of the AHM for different system sizes (the dashed line for $N=100$, and the solid line for $N=200$) in the U_A/t-U_B/t plane. The plot is symmetrical about the "line of homogeneity" $U_A=U_B$ which is shown by the dotted line.

IV. THE RENORMALIZATION GROUP CALCULATIONS

Next we apply a real space renormalization group (RG) technique[12] to the same model keeping in view the success of this technique to similar one-dimensional (1D) systems of correlated electrons[10,13,14] in the recent past. It is to be noted here that in order to achieve a closed parameter space under the present scheme of RG iteration, we must generalize the model (1) as follows:

$$H = \epsilon_A \sum_{i\in\mathcal{A}} n_i + \epsilon_B \sum_{i\in\mathcal{B}} n_i + t \sum_{i,\sigma} (c^\dagger_{i,\sigma} c_{i+1,\sigma} + \text{H.c.}) + U_A \sum_{i\in\mathcal{A}} n_{i,\uparrow} n_{i,\downarrow} + U_B \sum_{i\in\mathcal{B}} n_{i,\uparrow} n_{i,\downarrow}, \quad (5)$$

where, ϵ_A (ϵ_B) refers to the site energy of a site belonging to the $\mathcal{A}$ ($\mathcal{B}$) sublattice. We start with $\epsilon_A=\epsilon_B=0$ which makes (5) equivalent to (1). However, in the course of the RG iteration, nonzero values of ϵ_A and ϵ_B may appear.

When implementing the RG transformation the whole chain is now divided into cells containing three sites each. Since our system is a bipartite lattice with two types of sites A and B, there will appear two types of cells ABA and BAB. At the renormalized length scale, we identify the ABA cells as the new (renormalized) A-type sites and the BAB cells as the new B-type sites. There are four different on-site states for each site $|0\rangle$, $|+\rangle$, $|-\rangle$, $|+\ -\rangle$. We diagonalize the cell Hamiltonian (for both types of cells), and among the eigenstates of the cell Hamiltonian we retain only four low-lying states at each iteration, for construction of the RG recursion relations. We are interested in the half-filled ground state; so we retain the lowest energy states in the subspaces $\{n=2,\ S=S_z=0\}$, $\{n=3,\ S=\frac{1}{2},\ S_z=\pm\frac{1}{2}\}$, and $\{n=4,\ S=S_z=0\}$ of each type of cells. Here n, S, and S_z denote the total number of electrons, the total spin, and the z component of the total spin, respectively. These four states in a cell can now be identified as the renormalized on-site states $|0'\rangle$, $|+'\rangle$, $|-'\rangle$, and $|+-'\rangle$, respectively.

To find the renormalized hopping matrix element, the matrix elements of $c^b_\sigma(A)$ and $c^b_\sigma(B)$ between renormalized on-site states are calculated, where c^b_σ is the annihilation operator of the electron with spin σ at the boundary site of the cell and A or B in the parentheses denote the type of the cell. Let for an ABA-type cell

$$\langle 0'|c^b_\uparrow(A)|+'\rangle = \lambda_1(A),$$

$$\langle -'|c^b_\uparrow(A)|+-'\rangle = \lambda_2(A), \quad (6)$$

and for a BAB-type cell

$$\langle 0'|c^b_\uparrow(B)|+'\rangle = \lambda_1(B),$$

$$\langle -'|c^b_\uparrow(B)|+-'\rangle = \lambda_2(B). \quad (7)$$

Our system possesses spin-reversal symmetry, so the matrix elements for $c^b_\downarrow$'s will be the same as that of $c^b_\uparrow$'s (except for a fermionic sign change in the value of λ_2). But due to the lack of particle-hole symmetry, $\lambda_1(A)\neq\lambda_2(A)$ and $\lambda_1(B)\neq\lambda_2(B)$. At this stage we introduce an approximation[10,13,15] by defining

$$\lambda(A) = \sqrt{\lambda_1(A)\lambda_2(A)},$$

$$\lambda(B) = \sqrt{\lambda_1(B)\lambda_2(B)}, \tag{8}$$

which leads to

$$c_\sigma^b(\Gamma) = \lambda(\Gamma)c'_\sigma(\Gamma), \tag{9}$$

where $\Gamma = A, B$ and $\sigma = \uparrow, \downarrow$. So the effective renormalized hopping becomes

$$t' = \lambda(A)\lambda(B)t. \tag{10}$$

The intracell Hamiltonian, restricted to the subspace of the four states $|0'\rangle$, $|+'\rangle$, $|-'\rangle$, and $|+-'\rangle$, can now be written in terms of the new cell-fermion operators[12] as

$$H' = E_{0'} + (E_{+'} - E_{0'})(n'_\uparrow + n'_\downarrow) + (E_{+-'} + E_{0'} - 2E_{+'})n'_\uparrow n'_\downarrow, \tag{11}$$

where $E_{+-'}$, $E_{+'}$, and $E_{0'}$ are the lowest energies of the subspaces corresponding to four, three, and two particles, respectively. From this we can easily identify the renormalized on-site quantities

$$U'_\Gamma = E_{+-'}(\Gamma) + E_{0'}(\Gamma) - 2E_{+'}(\Gamma) \tag{12}$$

and

$$\epsilon'_\Gamma = E_{+'}(\Gamma) - E_{0'}(\Gamma), \tag{13}$$

where $\Gamma = A, B$.

The ground-state energy per site is computed from the sum

$$E_0 = \frac{1}{2}\sum_{n=1}^{\infty} \frac{[E_{0'}^{(n)}(A) + E_{0'}^{(n)}(B)]}{3^n}, \tag{14}$$

where n denotes nth stage of iteration. We also calculate the local moment L_0 defined by

$$L_0 = \tfrac{3}{4}(n_\uparrow - n_\downarrow)^2.$$

In absence of particle-hole symmetry this leads to a recursion relation of the form[10]

$$L_0 = a + bL'_0 + cP', \tag{15}$$

where, $P = (n_\uparrow + n_\downarrow)(n_\uparrow + n_\downarrow - 1)$ obeys a similar recursion relation given by

$$P = d + eL'_0 + fP', \tag{16}$$

with a, b, c, d, e, and f obtained from the matrix elements of L_0 and P between the truncated basis of the cell Hamiltonian. The operators L_0 and P are considered for the central site of the cell to minimize the boundary effects.[10,12] However, in implementing the recursion relation it is to be noted that a recursion for L_0 at a B-type site (being at the middle of an ABA cell) will involve L'_0 and P' pertaining to a renormalized A-type site, because under the RG transformation the ABA cell $\rightarrow$ a renormalized A site. Similar consideration arises for P as well. L_0 found for two different types of sites need not be equal to each other, in general.

To see the nature of the short-range spin correlation we further compute the nearest-neighbor (NN) spin-correlation function $\langle S_{1z}S_{2z}\rangle$, and the next-nearest-neighbor (NNN) spin-correlation function $\langle S_{1z}S_{3z}\rangle$ in each type of cell, where $S_{iz} = n_{i,\uparrow} - n_{i,\downarrow}$. Recursion relations are very much similar to that for L_0.

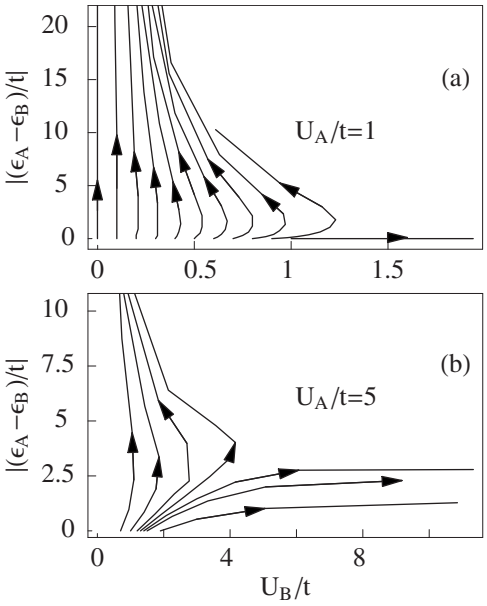

FIG. 4. RG flow diagram in an effective parameter space $U_B/t - |(\epsilon_A - \epsilon_B)/t|$ for (a) $U_A/t = 1.0$, and (b) $U_A/t = 5.0$. Point of repulsion of flow lines on the U_B/t axis identifies a transition point between two types of phases.

V. RESULTS OF RENORMALIZATION GROUP CALCULATIONS

We construct the phase diagram primarily by studying the RG flow pattern. We always start our iteration with $\epsilon_A = \epsilon_B = 0$ and U_A/t, $U_B/t \geq 0$. A transition point can be easily identified by looking into the RG flow diagram in the effective parameter space $\{U_B/t, |(\epsilon_A - \epsilon_B)/t|$ at a given value of U_A/t. For each value of U_A/t, there exists a point on the U_B/t axis (with $0 \leq U_B/t \leq U_A/t$) which behaves like a "point of repulsion" between the flow lines (Fig. 4). Starting from any point on its left-hand side the RG flow tends to go to the fixed point $\{0, \infty\}$, indicating a charge-ordered phase, while any point on its right flows to $\{\infty, 0\}$ indicating a spin-density wave. A plot of these transition points on the $U_A/t - U_B/t$ plane shows the phase boundaries, which can also be viewed as "lines of repulsion" of the flow diagram projected on the $U_A/t - U_B/t$ plane (Fig. 5). At this point it is interesting to find out the energy gap in the spectrum, Δ_{RG}, from the present RG calculation. For the present case we find that the Hamiltonian always flows under the RG iterations to fixed points corresponding to the "atomic limit" $(t \rightarrow 0)$ of (5) with parameters $\epsilon_A^{(\infty)}$, $\epsilon_B^{(\infty)}$, and $U_A^{(\infty)} = U_B^{(\infty)} = U^{(\infty)}$, where the superscript (∞) refers to the converged values of the corresponding parameters in (5). Therefore, the gap can be calculated from $\Delta_{RG} = |(|\epsilon_A^{(\infty)} - \epsilon_B^{(\infty)}| - U^{(\infty)})|$. We find that at the transition points the energy gap in the spectrum vanishes. In Fig. 6 we

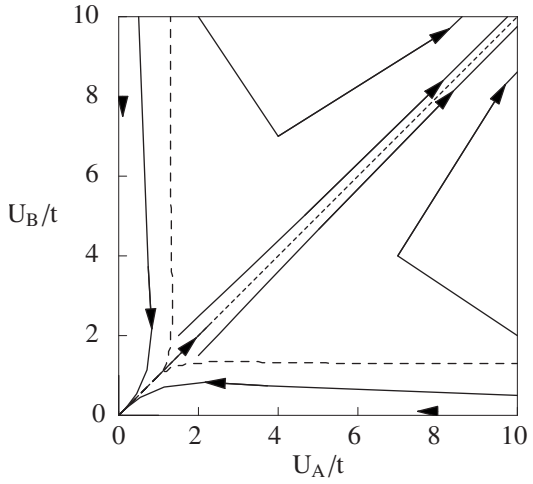

FIG. 5. RG flow diagram as projected on the U_A/t-U_B/t plane together with the phase boundaries (dashed lines) which seem to be the "lines of repulsion" of the flow lines. The "line of homogeneity" is shown by the dotted line.

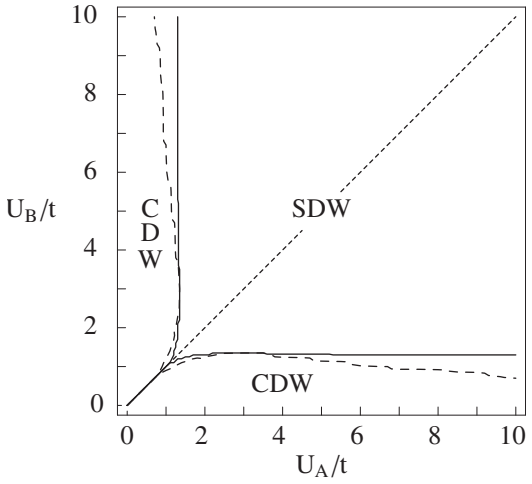

FIG. 7. Phase diagram obtained from the RG (solid line) superimposed on the HFA phase diagram (dashed line) in the U_A/t-U_B/t plane. The "line of homogeneity" is shown by the dotted line.

plot the energy gap Δ_{RG} as a function of U_B/t for different values of U_A/t. It is interesting to note that the zeroes of Δ_{RG} occur at values of U_A and U_B which are very close to the corresponding values obtained at zeroes of Δ_{HFA}. Therefore, the phase diagram obtained in the RG calculation agrees fairly well with that obtained in the HFA calculation (Fig. 7). Departures are appreciable only at the strong coupling limit; it can be easily understood because in this limit the error due to the truncation of basis becomes most serious in the present RG scheme for a model having two types of cells.[10] The energy scales used for truncation of basis in the two types of cells now become appreciably different; the RG result, therefore, may not be highly reliable in this sector. However, the agreement of the RG and the HFA results from the weak to the intermediate coupling regime really indicates that these results are very much reliable.

In Fig. 8 we plot the local moments at two types of sites as functions of U_B/t for different values of U_A/t. It turns out that L_0 is always higher at sites with larger values of Coulomb correlation. This is in agreement with a previous observation in Ref. 4. L_0 at A-type site equals that at B-type site only at the point of homogeneity, i.e., at $U_A=U_B$. It is rather interesting to note that the values of L_0 is slightly larger than $\frac{3}{8}$ even in the parameter space where, according to the RG flow pattern (and also from the HFA), the system develops a CDW instability. This shows that this correlation-driven CDW phase is dominated by short length-scale fluctuations that are suppressed in a CDW phase generated by a periodic modulation in the site potentials alone.[10]

We also calculate the NN and NNN spin-spin correlation functions with reference to *ABA*- and *BAB*-type cells. Plotted as functions of U_B/t these (Fig. 9) reveal some interesting

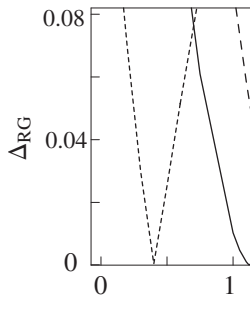

FIG. 6. Plot of the energy gap Δ_{RG}, as found from the RG calculation, against U_B/t. The dotted, solid, and the dashed lines correspond to $U_A=0.4$, 1.2, and 2.5, respectively (scale of energy is chosen by setting $t=1.0$).

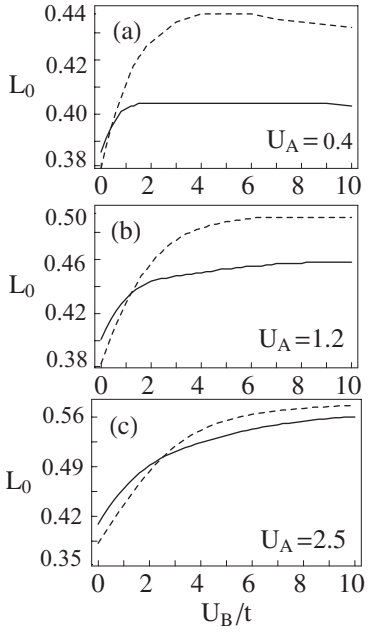

FIG. 8. Plot of the local moments L_0 as functions of U_B/t for (a) $U_A=0.4$, (b) $U_A=1.2$, and (c) $U_A=2.5$ (scale of energy is chosen by setting $t=1.0$). The solid line shows the data for the *ABA* block, and the dashed line shows the data for the *BAB* block. The curves cross over each other at the "point of homogeneity."

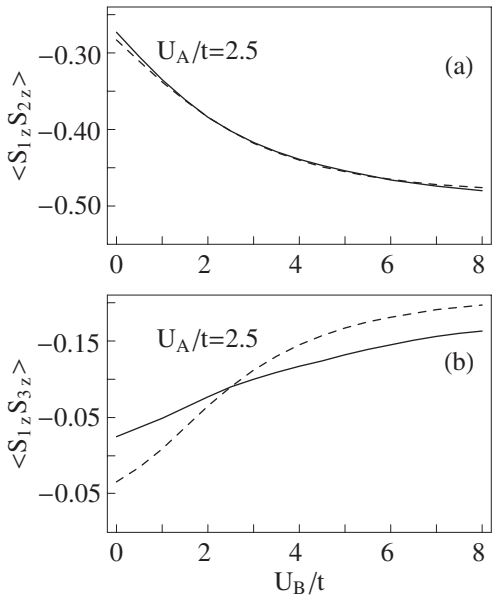

FIG. 9. Plot of the spin-spin correlation functions as functions of $U_B/t(U_A/t=2.5)$ for (a) NN correlation and (b) NNN correlation. The solid line shows the data for the *ABA* block, and the dashed line shows the data for the *BAB* block.

points. The negative value of $\langle S_{1z}S_{2z}\rangle$ indicates a nearest-neighbor antiferromagnetic alignment, which is increasing from the CDW to the SDW regime, as one should expect on physical grounds. That this correlation is not zero even within the CDW phase is really a reflection of the short-range fluctuations that we have just mentioned. However, the NN correlation has slightly different values in *ABA* and *BAB* cells. This difference, which is much more pronounced at higher values of $|U_A-U_B|$, is possibly related to the finite size effect of the RG. This effect is suppressed at weak coupling and near the "homogeneous" point in the SDW region. On the other hand, the NNN correlation has opposite signs for the *ABA*- and *BAB*-type cells in a region corresponding to the charge-density instability. This indicates a frustration that suppresses the large distance antiferromagnetic correlation. This frustration persists even within the SDW phase as it is evident from the widely different values of the NNN correlation in *ABA*- and *BAB*-type cells. Such an effect has already been anticipated in a previous work.[4] It is to be noted here that this effect gradually reduces as $U_B \to U_A$. In this respect the "SDW phase" of the half-filled AHM is behaving in a different way than the SDW instability found in a half-filled Hubbard model [the "homogeneous limit" of the present model (1)].

VI. STUDY OF MAGNETOCONDUCTANCE

Now we study the nature of the ground state of the superlattice structure in presence of a magnetic field. The magnetic field penetrating the ring will interact with the moments of the electrons. There will be an additive Zeeman term of the form $\mu_\sigma H'$ in the Hamiltonian (1), where μ_σ is the moment of the spin σ and H' is the penetrating magnetic field. The Hamiltonian now becomes

$$H = H'\sum_{i,\sigma}\mu_\sigma n_{i,\sigma} + t\sum_{i,\sigma}(c^\dagger_{i,\sigma}c_{i+1,\sigma} + \text{H.c.}) + U_A\sum_{i\in\mathcal{A}} n_{i,\uparrow}n_{i,\downarrow} + U_B\sum_{i\in\mathcal{B}} n_{i,\uparrow}n_{i,\downarrow}. \tag{17}$$

We follow the same HFA to decouple the Hamiltonian. Since we have found regions of the parameter space where the HFA results and the RG results match very well, we can rely on the HFA results in these regions. The Hamiltonian corresponding to the up- (down-) spin electrons will generate the up- (down-) spin band. These two bands are not degenerate because the spin-reversal symmetry is now broken. Therefore, at half filling, the number of up- and down-spin electrons will be different and a net moment will be generated.

For nonzero values of $U_A(>0)$ and $U_B=0$, the system is charge ordered at half filling in absence of a magnetic field. This is an insulating phase with a gap between the upper and lower bands; at half filling the lower bands for both spin species are totally filled. When a small magnetic field is turned on, the up- and down-spin bands shift in the opposite directions in energy scale. At a sufficiently large value of the magnetic field the upper band of the up-spin electrons tend to get occupied at the cost of depopulating the lower band of the down-spin electrons. Thus the ground state contains unequal number of up and down spins and the system, now having two partially filled bands, becomes conducting. If we go on increasing the magnetic field beyond a certain value, the said up-spin band will be completely filled while the down-spin band will be completely empty. The system is now spin polarized, leading again to an insulating phase. This can be easily checked by calculating the Drude weight[16] which measures the dc conductivity of the chain. Similar analysis can be made for $U_B \neq 0$ as well. Of course, in this case there arises a possibility of transition to a conducting phase from an SDW under the application of the field H'. We have calculated the Drude weight both for $U_B=0$ and $U_B=2$. To calculate the Drude weight, a vanishingly small magnetic flux Φ (in units of flux quantum $\phi_0=hc/e$) is introduced. The ring encloses this flux, but the flux does not penetrate the ring. Now the hopping term is modified by a phase factor. The Hamiltonian becomes

$$H = H'\sum_{i,\sigma}\mu_\sigma n_{i,\sigma} + t\sum_{i,\sigma}(c^\dagger_{i,\sigma}c_{i+1,\sigma}e^{2\pi i\phi} + \text{H.c.}) + U_A\sum_{i\in\mathcal{A}} n_{i,\uparrow}n_{i,\downarrow} + U_B\sum_{i\in\mathcal{B}} n_{i,\uparrow}n_{i,\downarrow}, \tag{18}$$

where $\phi=\Phi/N$, N being the number of sites in the ring. The Drude weight is calculated from the formula[10,17]

$$D = \frac{N}{4\pi^2}\left(\frac{\partial^2 E(\Phi)}{\partial\Phi^2}\right)_{\Phi=0}, \tag{19}$$

where $E(\Phi)$ is the ground-state energy of (18) calculated within the HFA.

We have plotted the Drude weight D against the penetrating magnetic field H' (Fig. 10) with $N=300$ for fixed set of values of U_A and U_B. The curves clearly show the transition between conducting and insulating phases. For lower and higher values of H' the Drude weight is zero, i.e., the system

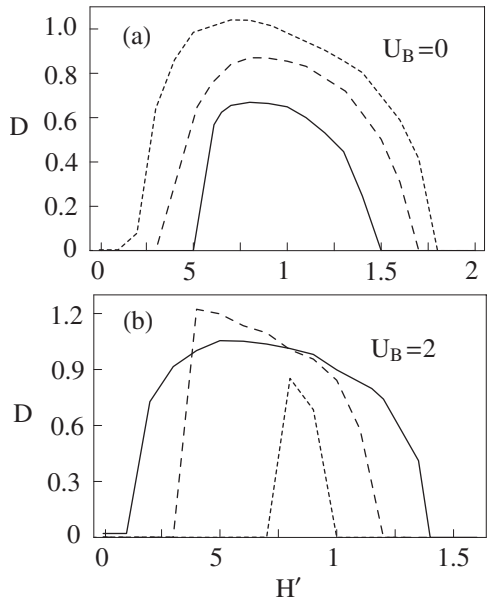

FIG. 10. Plot of the Drude weight D vs the field H' for (a) $U_B=0$. and (b) $U_B=2.0$. The dotted, dashed, and the solid lines correspond to $U_A=1.0$, 2.0, and 4.0, respectively, in (a), and to $U_A=3.0$, 2.0, and 0.9, respectively, in (b) (scale of energy is chosen by setting $t=1.0$).

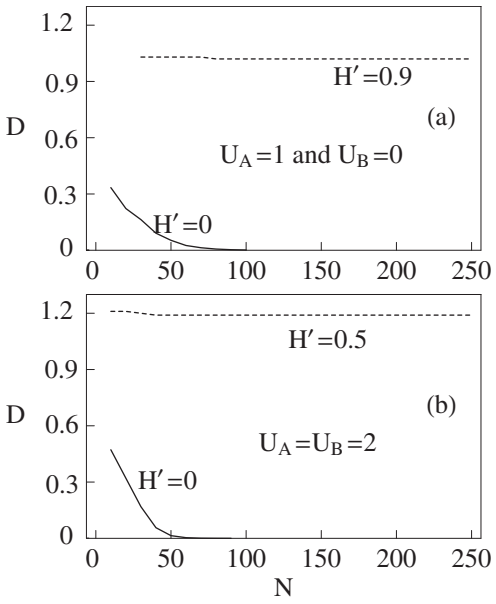

FIG. 11. Plot of the Drude weight D vs system size N for (a) $U_A=1.0$ and $U_B=0$, and (b) $U_A=U_B=2.0$ (scale of energy is chosen by setting $t=1.0$). Cases with $H'=0$ (solid line) and $H'>H'_c$ (dashed line) are shown where H'_c is the value of H' for which the system enters a conducting phase from an insulating one.

is insulating. But for moderate values of H' (depending on the value of on-site Coulomb repulsion energy), the Drude weight is quite large, implying a conducting phase. For higher values of U_A the conducting region becomes narrower. For different combinations of U_A and U_B values, we have plotted (Fig. 11) the Drude weight D against system size N. For the values of the penetrating magnetic field H', for which the upper band of the up-spins starts to depopulate and the lower down-spin band gets partially populated, the system goes to a conducting phase. In fact, the Drude weight remains unaltered as we increase the system size. For $H'=0$, the present system is found to be either in a CDW or in an SDW phase (Fig. 1) which is insulating. Therefore, the conductivity of such a system of macroscopic size must be vanishing. Thus in this region, the Drude weight falls sharply with increasing system size. Similar things happen for small values of H' for which the system is yet to pass on to the conducting phase. To identify the nature of the insulating phases directly, we study the spin- and charge-density parameters, s and c, respectively, together with the magnetization

$$m = \tfrac{1}{2}\langle n_{B,\uparrow} - n_{B,\downarrow} + n_{A,\uparrow} - n_{A,\downarrow}\rangle.$$

Figure 12 shows the plots of c, s, and m as functions of H' for different values of U_A and U_B. For $U_A \gg U_B$ we find that the increase in H' drives the system from a charge-ordered phase (large c) to a phase where c,s, and m are nearly comparable; this indicates the existence of a conducting state due to the absence of any kind of long-range ordering. We have already noted in Fig. 10 that in this region D is nonzero which is consistent with the above observation. Further increase in H' would completely depopulate the down-spin bands and consequently the up-spin bands would be filled up. This induces a sharp rise in m (together with a vanishing D) indicating a transition into an insulating spin-polarized phase. For $U_B \sim U_A(\sim t)$, however, the initial transition is from a spin-ordered phase to a metallic one. Thus we can construct the phase diagram (Fig. 13) of the AHM in

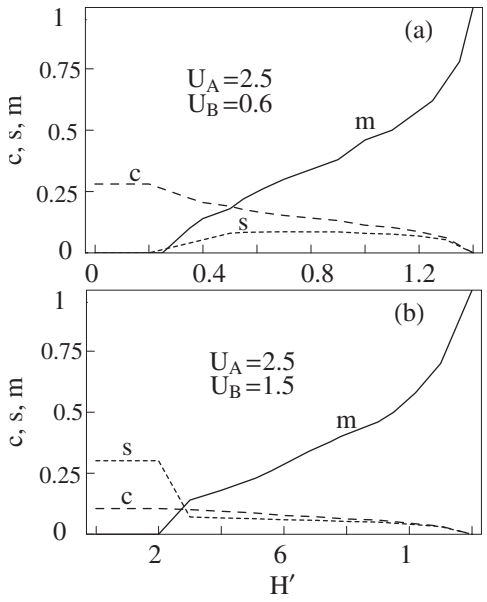

FIG. 12. Plot of the order parameters c, s, and m against the field H'. The solid line shows magnetization, the dotted line shows spin-order parameter, and the dashed line shows charge-order parameter for (a) $U_B=0.6$ and (b) $U_B=1.5$ while $U_A=2.5$ (scale of energy is chosen by setting $t=1.0$) and $N=100$.

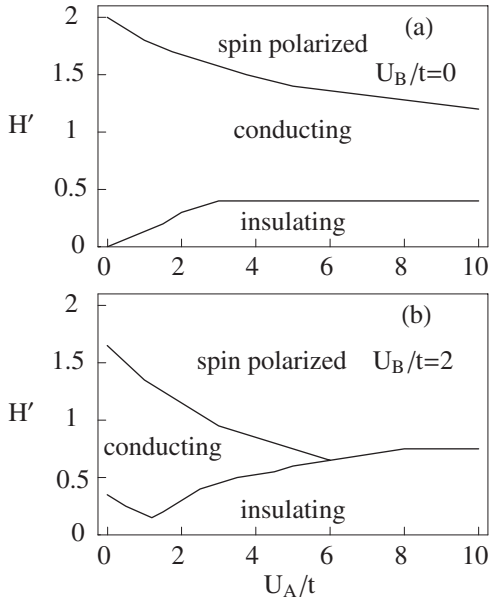

FIG. 13. The HFA phase diagram of the AHM in presence of a Zeeman field H' for $N=100$ and for (a) $U_B/t=0$ and (b) $U_B/t=2$.

the presence of a Zeeman field which shows the possibility of having an enhanced magnetoconductance for moderate values of the repulsive interactions. In case of very large Coulomb interaction, however, no conducting phase appears, and a direct transition from an insulating SDW phase to a spin-polarized phase is observed.

VII. CONCLUSION

Summarizing, we have investigated the one-dimensional half-filled alternating Hubbard superlattice structure at zero temperature using the Hartree-Fock approximation and a real space renormalization group technique. Although both methods are approximate ones, they are complementary to each other. The agreement between the phase diagrams obtained from these two different methods shows that the results are rather reliable. We obtained two types of phases, dominated by charge- and spin-density-wave instabilities, respectively, depending on the U_A and U_B values. The U_A-U_B phase diagram shows two transition lines, indicating a centrally located antiferromagnetic region and two charge-density-wave regions near the axes. The system is insulating. It may be noted at this point that the possibility of such transitions was not explored in the previous works on this model; most of these works concentrated only on a limited region of the parameter space, e.g., $U_A>0$ and $U_B=0$, and also there were some severe restrictions on the system size. Apart from the phase transitions, it is interesting to note that there appears a spatial modulation of the local moments dictated by the inhomogeneity of the correlation parameters. The RG results also indicate that the ordering is not full grown as compared to the homogeneous limit because of underlying frustration of spin-spin correlation. These results are in agreement with a previous finding.[4] Also we have studied the ground-state properties, including the Drude weight, of the superlattice in the presence of a magnetic field (H'). The U_A-H' (for fixed U_B) phase diagram shows that the system becomes conducting for an intermediate range of values of H'. In the phase diagram, we obtained insulating phases for lower and higher values of H'. The width of the conducting region depends on the values of on-site Coulomb repulsion energies of the superlattice structure. It seems interesting to explore this model further, especially at finite temperatures and for cases away from half filling. Also the effect of varying "spacer thickness"[4–6] for this regime of correlation parameters may yield some interesting observations.

ACKNOWLEDGMENT

Two of the authors (J.C. and B.B.) sincerely acknowledge a fruitful discussion with Shreekantha Sil.

[1] B. Heinrich and J. F. Cochran, Adv. Phys. **42**, 523 (1993).
[2] S. S. P. Parkin, N. More, and K. P. Roche, Phys. Rev. Lett. **64**, 2304 (1990); S. S. P. Parkin, *ibid.* **67**, 3598 (1991); P. Grünberg *et al.*, J. Appl. Phys. **69**, 4789 (1991).
[3] M. N. Baibich, J. M. Broto, A. Fert, F. Nguyen Van Dau, F. Petroff, P. Etienne, G. Creuzet, A. Friederich, and J. Chazelas, Phys. Rev. Lett. **61**, 2472 (1988).
[4] T. Paiva and R. R. dos Santos, Phys. Rev. Lett. **76**, 1126 (1996); Phys. Rev. B **62**, 7007 (2000).
[5] T. Paiva and R. R. dos Santos, Phys. Rev. B **58**, 9607 (1998).
[6] T. Paiva and R. R. dos Santos, Phys. Rev. B **65**, 153101 (2002).
[7] A. L. Malvezzi, T. Paiva, and R. R. dos Santos, Phys. Rev. B **66**, 064430 (2002); Phys. Rev. B **73**, 193407 (2006).
[8] J. Silva-Valencia, E. Miranda, and R. R. dos Santos, J. Phys.: Condens. Matter **13**, L619 (2001); Phys. Rev. B **65**, 115115 (2002).
[9] P. Kakashvili and G. I. Japaridze, J. Phys.: Condens. Matter **16**, 5815 (2004).
[10] S. Gupta, S. Sil, and B. Bhattacharyya, Phys. Rev. B **63**, 125113 (2001); **64**, 169903 (2001).
[11] H. Shiba, Phys. Rev. B **6**, 930 (1972).
[12] J. E. Hirsch, Phys. Rev. B **22**, 5259 (1980).
[13] B. Bhattacharyya and S. Sil, Phys. Lett. A **180**, 299 (1993).
[14] B. Bhattacharyya and G. K. Roy, J. Phys.: Condens. Matter **7**, 5537 (1995); B. Bhattacharyya and S. Sil, *ibid.* **11**, 3513 (1999).
[15] M. Ma, Phys. Rev. B **26**, 5097 (1982).
[16] W. Kohn, Phys. Rev. **133**, A171 (1964).
[17] S. Gupta, S. Sil, and B. Bhattacharyya, Physica B **355**, 299 (2005).